Research Square

Preprints are preliminary reports that have not undergone peer review.
They should not be considered conclusive, used to inform clinical practice,
or referenced by the media as validated information.

HSC70、HSPA1A, and HSP90AB1 Facilitate Ebola Virus trVLPs to Induce Chaperone-Mediated Autophagy

DONGSHAN YU
The Second Affiliated Hospital of Nanchang University
Shu-Hao Yao
Wenzhou Medical University Renji College
Wen-Na Xi
The Second Affiliated Hospital of Nanchang University
Lin-Fang Cheng
Zhejiang University School of Medicine
Fu-Min Liu
Zhejiang University School of Medicine
Haibo Wu
Zhejiang University School of Medicine
Xiang-Yun Lu
Zhejiang University School of Medicine
Nan-Ping Wu
Zhejiang University School of Medicine
SHUILIN SUN
The Second Affiliated Hospital of Nanchang University
Hang-Ping Yao (yaohangping@zju.edu.cn)
Zhejiang University School of Medicine

Research Article

Keywords: EBOV, trVLPs, chaperone-mediated autophagy, HSC70, HSPA1A, HSP90AB1

Posted Date: August 18th, 2023

DOI: https://doi.org/10.21203/rs.3.rs-3173559/v1

License: This work is licensed under a Creative Commons Attribution 4.0 International License. Read Full License

Additional Declarations: No competing interests reported.

Abstract

Background

Ebola virus (EBOV) can induce autophagy to benefit the virus life cycle, but detailed mechanisms remain to be elucidated. We previously found that EBOV GP and VP40 proteins interact with host chaperones, including HSC70 (HSPA8), HSPA1A, and HSP90AB1, which are probably associated with chaperone-mediated autophagy (CMA).

Methods

We developed EBOV-trVLPs to model the EBOV life cycle, infected 293T cells with trVLPs, evaluated CMA by GFP-LC3 and RFP-LAMP1 co-localization, transmission electron microscopy (TEM) observation, and immunoblot analysis.

Results

The data suggest that EBOV-trVLPs may induce autophagy via CMA, but are not constrained by the CMA pathway. HSC70, HSPA1A and HSP90AB1 participate in and regulate the CMA induced by EBOV-trVLPs.

Conclusions

This is the first study of CMA induced by EBOV-trVLPs and provides insight into viral-host interactions that are presumably related to CMA.

1. Introduction

Ebola virus (EBOV) is a single-stranded, negative-sense RNA virus that was first reported in 1976 to be the cause of the highly contagious zoonotic disease and Ebola viral disease (EVD) in humans and other primates [1]. Five different subtypes of EBOV have been defined: 1) Ebola virus (EBOV, previously known as Zaire ebolavirus); 2) Sudan virus (SUDV); 3) Bundibugyo virus (BDBV); 4) Taï Forest virus (TAFV); and 5) Reston virus (RESTV) [2]. The EVD epidemic from December 2013 to March 2016 in Western Africa was caused by EBOV and was associated with > 28,000 cases and > 11,000 deaths in 11 countries [3]. In 2019, the ongoing EVD epidemic was significantly expanded and was associated with a high fatality rate of 67% from 2018 to 2019 in the democratic public of the Congo[4]. Even now, the ongoing challenge of EVD epidemic in the democratic public of the Congo indicated a great potential of re-emergence of the epidemic, especially coupled with the emergence of COVID-19, jeopardizing the health system's response to outbreak[5].

Although numerous studies have been devoted to EVD therapeutics, the pathogenesis, molecular mechanisms, and EBOV-host interactions are still poorly understood. EBOV-induced autophagy is an area where the mechanism of association remains unclear. Autophagy is the process responsible for the degradation and recycling of damaged organelles through lysosomal degradation [6]. Under conditions of cellular stress (e.g., nutrient deficiency, virus infection, and chemotherapy), autophagy can be initiated through different mechanisms and affect the survival of virally-infected or transformed cells [7–9]. There are at least three types of autophagy: 1) macroautophagy; 2) microautophagy; and 3) chaperone-mediated autophagy (CMA) [10]. CMA is a selective degradation pathway with distinctive mechanisms for cargo recognition and internalization into the lysosome. Meanwhile, CMA is initiated by the recognition of cytosolic heat shock cognate protein of 70 kDa (HSC70) to a consensus pentapeptide motif (KFERQ-like motif) [11, 12]. a group of co-chaperones, including HSP90, BAG-1and Hip, then form a complex of HSC70/KFERQ-containing proteins. The HSC70/KFERQ-protein complex targets the lysosome by binding to lysosome-associated membrane protein type 2A (LAMP-2A), which is recognized as an HSC70 receptor, and is then transported through the membrane and is degraded in the lysosomal lumen [13–15].

Currently, three possible mechanisms are considered to be involved in virus-induced autophagy: 1) double-stranded RNA induces autophagosome formation by reducing PKR activity and the downregulation of mTOR; 2) virus infection induces autophagosome formation through ER stress; and 3) a virus infection activates mTOR and accelerates cellular translation [11, 16, 17]. To date, the connection between EBOV and autophagy remains poorly understood. It has been reported that the BCL2-associated athanogene-3 (BAG-3) WW-domain can interact with the PPxY motif of both EBOV and MARV VP40, negatively regulates the budding of VP40 VLPs and infectious virus [18]. Knockout of FAM134B, an autophagy receptor, resulted in inhibition of replication of the Ebola virus Strains, Makona and Mayinga[19]. Suppression of MTORC1 signaling by rapamycin activates autophagy and blocks filovirus egress. However, the detailed mechanisms of how EBOV induces autophagy remain to be elucidated.

In our previous studies, we found that the EBOV GP protein interacts with HSC70 (HSPA8), HSPA1A, and HSP90AB1; the EBOV VP40 protein and nucleic acids both interact with HSPA1A and HSP90AB1[20]. Based on the above researches, we hypothesize that EBOV may likely induce

autophagy via viral protein-host HSC70 or co-chaperon interactions via CMA in some as yet undefined pathway. We produced transcription- and replication-competent virus-like particles (trVLPs) to model the EBOV life cycle under biosafety level 2 conditions [21], assessed autophagy induced by trVLPs, evaluated CMA based on the co-localization of microtubule-associated protein light chain 3 (LC3) and lysosome-associated membrane glycoprotein 1 (LAMP1). We also used transmission electron microscopy (TEM) observations and immunoblot analysis to assess EBOV-trVLPs and host elements involved in the autophagy and CMA pathways. This is the first study of the lifecycle and CMA pathway of EBOV-trVLPs.

2. Materials and Methods

2.1. Cell Lines and Plasmids

Human embryonic kidney (HEK) 293T cells were cultured in Dulbecco's modified Eagle's medium (DMEM; Thermo Fisher, Waltham, MA, USA; Cat#10566016) containing 10% foetal calf serum (FBS; Gibco, Waltham, MA, USA; Cat#10099141), 2 mM L-glutamine (Life Technologies, Waltham, MA, USA; Cat#25030081), and 1% penicillin- streptomycin (Life Technologies; Cat#10378016) at 37°C with 5% CO_2. Plasmids pCAGGS-VP30, pCAGGS-VP35, pCAGGS-NP, pCAGGS-L, p4cis-vRNA-RLuc, pCAGGS-Tim1, and pCAGGS-T7 were kindly provided by Drs. Heinz Feldmann and Thomas Hoenen, Rocky Mountain Laboratories, National Institute of Health. GFP-LC3 (Addgene, Watertown, MA, USA; Cat# 11546) and RFP-LAMP1 (Addgene, Cat# 1817) were purchased from Addgene company.

2.2. Production of trVLPs

Producer 293T cells (p0) in six-well plates were transfected with plasmids encoding each EBOV structural protein (75 ng pCAGGS-VP30, 125 ng pCAGGS-VP35, 125 ng pCAGGS-NP, 1,000 ng pCAGGS-L, and 250 ng p4cis-vRNA-RLuc), and pCAGGS-T7 (250 ng) encoding a Renilla luciferase reporter [21]. Cellular supernatants (200 mL) from 10 six-well plates containing released trVLPs were harvested at 72 h post-transfection, and the cell debris was pelleted by centrifugation at 175 × g. The supernatant was then used to infect target 293T cells (p1) previously transfected with ribonucleoprotein (RNP) components (125 ng pCAGGS-NP, 125 ng pCAGGS-VP35, 75 ng pCAGGS-VP30, 1,000 ng pCAGGS-L, and 250 ng pCAGGS-Tim1) [20]. Target 293T cells (p2 – p5) were treated in a similar manner. Cleared supernatants (33 mL) in 2 mL of 20% sucrose from the bottom of each tube were centrifuged at 125,000 × g in a SW-28 rotor for 3 h at 4°C. The resulting pellets were resuspended in 100 µL ice-cold NTE buffer (10 mM Tris pH 7.5, 100 mM NaCl, and 1 mM EDTA) by tapping gently approximately 100 times, and trVLPs were stored on ice or in a refrigerator at 4°C until further use.

2.3. Imaging of the DiI-labeled trVLPs internalization in live 293T cells

The trVLPs were suspended in 1 ml of NTE buffer, and 1,1'-Dioctadecyl-3,3,3',3'-Tetramethylindocarbocyanine Perchlorate (DiI, final concentration:10 µM, Invitrogen, Waltham, MA, USA, Cat# D282) was added and thoroughly mixed. The mixture was gently shaken at room temperature for 1 h and then filtered through a strainer (0.22 µm pore size; Millipore, Darmstadt, Germany, Cat#SLGP033RB). 293T cells cultured in 8-well Chamber Slides with removable wells were incubated with the DiI-labeled trVLPs at 4°C for 10 min, washed with PBS, and warmed at 37°C. Then, 4',6-diamidino-2-phenylindole (DAPI, diluted by PBS in 10 µg/ml, Invitrogen, Waltham, MA, USA, Cat#P36931) was added to stain the nucleus. Later, the well was set on the stage of a fluorescence microscope, the internalization process of DiI-labeled trVLPs in 293T cells was imaged at different time points.

2.3. TCID50 and MOI of trVLPs

TrVLPs infectivity titre was titrated using 50% tissue culture infective dose (TCID50). TrVLPs were diluted at 10-fold serially with DMEM from 10^{-1} to 10^{-10} concentrations. The attenuated trVLPs (100 µl) were added to wells in each row of a 96-well plate, and 293T cell suspension (100 µl) was added to each well to a final cell density of 2×10^5 cells/ml. 293T cells without HP001 infection were included as controls. Cytopathic effects (CPEs) were observed by microscopy and recorded each day for 7 days, the results were used to calculate TCID50 by the Reed-Muench method[22]. The MOI value was calculated according to the equation MOI = 0.7×TCID50/ cell numbers (Table 1).

2.4. Electron Microscopy (EM) Analysis of trVLPs

trVLPs were pipetted onto a 300-mesh copper grid coated with carbon film, incubated for 5 min at room temperature, and the grids were washed twice with distilled water and negatively stained for 15 s with 1% uranyl acetate. The excess liquid was removed with a filter paper and trVLPs were visualized under a Hitachi H7000 transmission electron microscope.

2.5. Immunofluorescence

The 293T cells cultured in 24-wells plates were divided into groups, transfected with plasmids GFP-LC3 (800 ng/well), or GFP-LC3 plus LAMP1-RFP (400 ng/well each) respectively. 24 h post-transfection, the cells were treated with trVLPs (MOI = 1.5), or rapamycin (0.5 nM), or trVLPs (MOI = 1.5) plus 3-MA (0.5 nM) respectively. At 48 h after trVLPs infection or drug treatment, the GFP-LC3 and LAMP1-RFP dot formations were

detected under a fluorescence microscope (DMi8-M, Leica, German). The cells containing ≥ 5 GFP-LC3 dot formation were defined as autophagy-positive cells [23].

2.6. TEM Analysis of Autophagy

At 48 h after infection or treatment, the cells were collected and fixed in 2.5% glutaraldehyde in 0.1 M PBS for at least 4 h or overnight at 4°C. Later, the specimens were treated with 0.1% OsO_4 solution buffered in 0.1 M PBS for 2 h, dehydrated in a graded series of ethanol, and embedded in epoxy resin 812. Ultrathin sections of the specimens were collected on copper grids, double-stained with uranyl acetate and lead citrate, and examined by transmission electron microscopy (H-7000, Hitachi, Hitachinaka, Japan).

2.7. Western blot analysis

The total protein from 293T cells was extracted using RIPA extraction buffer (Beyotime, Shanghai, China, Cat# P0013K) with PMSF protease inhibitor (Solarbio, Beijing, China, Cat# P6730). The protein concentration was then quantified using the bicinchoninic acid (BCA) method (Sigma, Santa Clara, CA, USA, Cat# BCA1-1KT). The extract was eluted with 2× sodium dodecyl sulfate (SDS) loading buffer and resolved by SDS-polyacrylamide gel electrophoresis (PAGE). The proteins were transferred to polyvinylidene fluoride (PVDF) membranes, incubated with the sequential addition of the relevant primary and secondary antibodies, and detected with the Super Signal West Pico chemiluminescent substrate (Thermo Fisher; Cat# 34580). Moreover, to check siRNA interference with the expression of target proteins in a specific manner, an immunoblot analysis of the target host proteins was performed following siRNA transfection. GAPDH was used as the internal control. When immunoblot analysis was performed with lysosomal samples, the level of LAMP2 protein was used as an internal control.

2.8. Antibodies

Antibodies recognizing LC3B (Cat# 3868S), Phospho-mTOR(Cat# 5536S), Phospho-Akt (Cat# 4060S), HSPA1A (HSP70; Cat# 4873S), LAMP1 (Cat# 15665s), LAMP2 (Cat# 49067S), GAPDH (Cat# 2188), HRP-linked anti-rabbit IgG (Cat# 7074S), and HRP-linked anti-mouse IgG (Cat# 7076S) were purchased from Cell Signalling Technology (Danvers, MA, USA). Rapamycin (Cat# 1912) and 3-Methyladenine (3-MA, Cat# 3977) were purchased from R&D Systems (Minneapolis, MN, USA). HSC70 (HSPA8, Cat# NBP2-12880) and HSP90AB1 (Cat# NB110-61640) were purchased from Novus Biologicals (Littleton, CO, USA). PHLPP1 (Cat# MBS151247) was obtained from MyBioSource company (San Diego, CA, USA).

2.9. SiRNA knockdown

SiRNAs targeting HSC70, HSPA1A and HSP90AB1 were designed and synthesized with three siRNA sequences for each one, the most efficient sequence for RNA interference (RNAi) was evaluated by qPCR and were chosen for tests (Table 2). Meanwhile, cytotoxity of siRNAs were estimated by nuclei counting, the siRNA was classified as hypotoxicity if 75 or more nuclei within one vision of microscope (40×, 0.24mm^2) (Supplementary Fig. 1). In 24-well plates, 100 µL of opti-MEM medium (Invitrogen; Cat# 31985070) containing 1.4 µL siRNA and 4.5 µL HiPerFect transfection reagent (Qiagen, Dusseldorf, Germany; Cat# 301705) was added to each well, and the plates were shaken gently for 1 min. After a 10 min incubation at room temperature, a cell suspension (400 µL) containing 1 × 10^5 cells were added to obtain a final siRNA concentration of 75 nM. The cells were incubated at 37°C and 5% CO_2 for 48 h.

2.10. Lysosome Isolation

Lysosomes were purified from 293T cells using a lysosome isolation kit (Sigma, Cat# LYSISO1-1KT). According to the protocol, 1 × 10^8 293T cells were collected and the cell membranes were disrupted by ultrasound. The breakage was evaluated by staining with Trypan blue. The specimen was then serially centrifuged at 1,000 × g and 20,000 × g. The pellet was collected, and calcium chloride was later added to 8 mM, incubated for 15 min at room temperature, centrifuged at 5,000 × g, and the supernatants that contained lysosomal matrices were collected.

2.11. Statistical analysis

Data that exhibited a normal distribution were presented as the mean ± standard deviation. Student's *t*-tests (two-tailed, paired or unpaired t-tests with Welch's correction) were performed where appropriate. All analyses were performed with GraphPad Prism 5 (GraphPad Software, UK) and differences between the group means with $p < 0.05$ were considered statistically significant.

3. Results

3.1. EBOV-trVLPs could strongly mimic the wild type Ebola virus strain

EBOV-trVLPs exhibited a filamentous-like morphology with a major axis that was approximately 100 nm-1000 nm and a diameter of about 50 nm as visualized by EM (Fig. 1A-D). Meanwhile, DiI-labeled trVLPs in live 293T cells were visualized by fluorescent microscopy which indicated trVLPs could translocated into the cytoplasm (Fig. 1E). The images indicated that trVLPs could simulate the wild type strain in morphology, size, and basic functions to the greatest extent [24].

3.2. EBOV-trVLPs induced autophagy in 293T cells

Autophagy was observed in 293T cells 48 h after infection with trVLPs. As shown in Fig. 2A, cells containing GFP-LC3 puncture structures, which are used to monitor the number of autophagosomes, dominate among GFP-LC3-transfected cells. At a high magnification, the punctate dots were rich in these cells (≥ 5 dots/cell) (Fig. 2B -C). Moreover, we investigated the GFP-LC3-I and GFP-LC3-II proteins extracted from the cells by immunoblotting with antibodies against LC3 (Fig. 2D). The results indicate that cells that are induced by rapamycin or infected with trVLPs exhibit significant GFP-LC3-II expression, and that the transition from GFP-LC3-I to GFPLC3-II indicates the process of autophagy. Cells previously treated with 3-MA and subsequently infected with trVLPs also showed substantial GFP-LC3-II expression, suggesting that 3-MA is not effective in inhibiting autophagy induced by trVLPs. 3-MA is one of the most commonly used pharmacological approaches to inhibit class I PI3-kinase (PI3-K) and class III PI3 kinase activity which is required for autophagy [25]. The results suggest that trVLPs are likely to induce autophagy via other means and are not limited to the PI3-K/AKT/mTOR pathway.

Thus, based on previous findings, including: 1) trVLPs could induce autophagy; 2) 3-MA could not significantly inhibit autophagy induced by trVLPs; 3) trVLPs GP, VP40 protein, and nucleic acids have been shown to interact with HSC70 and co-chaperones; and 4) GP and VP40 proteins have critical roles in the EBOV-trVLPs life cycle (e.g., virus entry, uncoating, fusion and budding processes), we presumed that trVLPs probably induced autophagy via the CMA pathway to benefit viral production. To demonstrate this hypothesis, we evaluated the autophagy by co-localization of LAMP1 and LC3 fluorescence, TEM observations, and an immunoblot analysis.

3.3. EBOV-trVLPs induced autophagy via the CMA pathway

According to the protocol, 293T cells previously transfected with GFP-LC3 and RFP-LAMP1 were infected with EBOV-trVLPs. At 48 h post-infection, the co-localization of LC3 and LAMP1 was checked (Fig. 3A and B), since LAMPs (e.g., LAMP1 and LAMP2) are lysosomal proteins and used as endosome and lysosome markers, RFP-LAMP1 can be found at the early stage of autophagolysosome formation during autophagy; moreover, GFP-LC3 was able to bind to autophagosomes and autolysosomes [26, 27]. Thus, the RFP-LAMP1-positive dots (red) represent lysosomes and autophagolysosomes; GFP-LC3-positive dots (green) indicate autophagosomes and autolysosomes; and the co-localization of RFP-LAMP1 and GFP-LC3-positive dots (yellow) indicate autolysosomes, which suggest the maturation of autophagy induced by the CMA pathway. Moreover, we investigated 293T cells infected with trVLPs for 48 h by TEM (Fig. 3C – H). In Fig. 3C, E, and G, autophagosomes (indicated by a single arrow) and autolysosomes (indicated by double arrows) are obviously visible in the cytoplasm. Figure 3D and F clearly show autophagosomes fused with lysosomes to form autolysosomes (indicated by double arrows).

Meanwhile, to confirm the expression of CMA related proteins, phosphorylated mTOR(P-mTOR) and Phosphorylated Akt (P-Akt) from cell lysates, HSPA1A and PHLPP1 from lysosomes were subjected to immunoblot analysis with related antibodies. The data indicated that P-mTOR was significantly lower in the cells treated with trVLPs or rapamycin compared to untreated cells. Cells treated with either trVLPs or trVLPs plus 3-MA showed no significant change in P-mTOR expression. P-Akt was associated with a highly similar trend with P-mTOR (Fig. 3I). In the lysosome, HSPA1A was enriched in both trVLPs and trVLPs plus 3-MA treatment groups but appeared thin in the rapamycin and normal groups. PHLPP1 was substantially expressed in the trVLPs, rapamycin, and trVLPs plus 3-MA groups, compared with the normal cells (Fig. 3J). Meanwhile, we confirmed the results by immunoblot analysis. As Fig. 3K and M showed, the expression of P-mTOR and P-Akt in cell lysates were significantly lower in the trVLPs, rapamycin, trVLPs plus 3-MA groups compared to the normal group. By the way, P-mTOR and P-Akt got no distinct changes between trVLPs and trVLPs plus 3-MA groups. Lysosomal HSC70 and PHLPP1 were similar enriched in the trVLPs and trVLPs plus 3-MA groups, but thin in the rapamycin and normal groups (Fig. 3L and N). These results indicate that the Akt/mTOR/PHLPP1 axis is a common pathway for autophagy. In addition, lysosomes contribute to the CMA pathway and the level of lysosomal HSPA1A is proportional to the level of CMA activity. To confirm that trVLPs may induce autophagy via chaperone or co-chaperone-related lysosomal activity, we knocked out HSC70, HSPA1A, and HSP90AB1, which revealed interactions with either trVLPs GP or VP40 proteins, and then examined their effect on CMA.

3.4. TrVLPs-induced autophagy could be modulated by chaperone or co-chaperone-mediated pathways

Following the protocol, we knocked down HSC70, HSPA1A, and HSP90AB1 in 293T cells by siRNAs, respectively, and infected the cells with trVLPs for 48 h. The knockdown efficiency of the siRNAs was verified in Fig. 4A. The expression of the GFP-LC3, P-mTOR, and P-Akt proteins was examined in the cell lysates. These data indicate that a knockdown of HSC70, HSPA1A, and HSP90AB1 could significantly inhibit the conversion of GFP-LC3-I to GFP-LC3-II but have little effect on P-mTOR and P-Akt (Fig. 4B). In addition, the knockdown of HSC70, HSPA1A, or HSP90AB1 could eliminate lysosomal HSC70, but had no effect on lysosomal PHLPP1 (Fig. 4C). The data also demonstrate that a knock-down of HSC70 and associated co-chaperones may inhibit autophagy associated with trVLPs; However, there was no effect on the universal prodrug molecules, including mTOR, Akt and PHLPP1.These findings suggest that trVLPs are likely to induce autophagy by several means, and are not limited to the CMA route.

4. Discussion

To date, EBOV-induced cytopathies, including cellular necrosis, apoptosis, autophagy, and pyroptosis, are in urgent need of further elucidation. Although EBOV has been shown to cause autophagy, the detailed mechanism remains unclear. In autophagy, Akt and mTOR represent the major autophagy-inhibitory molecules, which play an important role in the autophagy signaling pathway and are regulated by a variety of signals; P-mTOR and P-Akt are sensitive markers for assessing autophagy [28, 29].

In this study, we observed that EBOV-trVLPs infection significantly induced autophagy. Even pre-treatment with 3-MA, an inhibitor of class III PI3-K, failed to inhibit autophagy induced by trVLPs. Since the PI3-K/Akt/mTOR pathway is a common pathway of attack, this result suggests that it is likely that trVLPs induce autophagy by other means and are not limited to the PI3-K/Akt/mTOR pathway. In our previous study, we confirmed that the EBOV-trVLPs GP proteins interact with HSC70, HSPA1A and HSP90AB1; moreover, viral nucleic acids and VP40 protein can both interact with HSPA1A and HSP90AB1 [20]. From this, we hypothesize that trVLPs are most likely induced autophagy by a chaperone- or co-chaperone-induced pathway. We assessed autophagy by the co-localization of RFP-LAMP1 and GFP-LC3 fluorescence and examined autophagy structures via TEM. Both fluorescence images and TEM revealed autolysosome formation. Moreover, the significantly lower expression of P-Akt and P-mTOR in the cell lysate, and the high expression of PHLPP1 and HSC70 in the lysosome from trVLPs and trVLPs plus the 3-MA group strongly suggest that trVLPs infection may induce autophagy via the CMA pathway but is not restricted to this pathway.

The CMA is initiated by the binding of HSC70 to the substrate; however, a successful CMA process requires a series of coordinated events from other molecules, including co-chaperones and receptors [30]. It has been reported that a blockage of HSC70 co-chaperones present on the lysosomal surface could reduce substrate translocation, although the specific contribution of co-chaperones remains unclear [31]. Moreover, lysosomal HSP90, which localizes to both the cytosolic and luminal sides of the lysosome, facilitates LAMP2A stabilization as it transitions through different stages [14, 30].

In siRNA interference tests, knockout of HSC70, HSPA1A, and HSP90AB1 were shown to suppress autophagy and lysosomal HSC70 levels, respectively; However, the P-Akt, P-mTOR and PHLPP1 proteins were not affected. This data demonstrated that: 1) the downregulation of HSC70 and co-chaperons could inhibit the CMA pathway but was negative to other autophagy pathways; 2) co-chaperons probably play an indispensable role in the CMA process; 3) low-levels of HSC70 and co-chaperons can possibly affect the viral protein-host protein interactions and further impair the trVLPs life cycle, which may indirectly affect the CMA.

There are limitations associated with our study. First, the tests are based on EBOV-trVLPs, which may not reflect the physiology of a live EBOV; Therefore, the results need to be confirmed under realistic EBOV conditions. Second, in addition to CMA, we did not carefully examine other autophagy pathways likely induced by trVLPs. Finally, which of the trVLPs proteins primarily induces the CMA pathway and the detailed mechanism remain unclear. In subsequent experiments, we will attempt to define the viral proteins of trVLPs that induce CMA, elucidate the mechanisms, and relate these mechanisms to the lifetimes of trVLPs.

In summary, we have demonstrated that infection with EBOV-trVLPs can induce autophagy via CMA, but do not restrict ourselves to this approach. In the CMA, the co-chaperones are likely to play an integral role. Moreover, it can be conjectured that the GP or vp40 protein-host protein interactions of trVLPs may affect autophagy, which may be relevant for the viral life cycle.

Abbreviations

BAG-3, BCL2 associated athanogene-3;

BCA, Bicinchoninic acid;

BDBV, Bundibugyo virus;

CMA, Chaperone-mediated autophagy;

DiI, 1,1'-dioctadecyl-3,3,3',3'-tetramethylindocarbocyanine perchlorate;

DMEM, Dulbecco's modified Eagle's medium;

EBOV, Ebola virus;

EVD, Ebola viral disease;

ER, Endoplasmic reticulum;

EM, Electron Microscopy;

FBS, Foetal calf serum;

HEK, Human embryonic kidney;

HSC70, Heat shock cognate protein of 70 kDa;

LAMP1, lysosome-associated membrane glycoprotein 1;

LC3, microtubule-associated protein light chain 3;

PAGE, Gel electrophoresis;

P-Akt, Phosphorylated Akt;

P-mTOR, phosphorylated mTOR;

RESTV, Reston virus;

RNP, Ribonucleoprotein;

SUDV, Sudan virus;

TAFV, Taï Forest virus;

TEM, Transmission electron microscopy.

Declarations

Ethics approval and consent to participate

Not applicable.

Consent for publication

The Author confirms: that the work described has not been published before; that it is not under consideration for publication elsewhere; that its publication has been approved by all co-authors, if any; that its publication has been approved by the responsible authorities at the institution where the work is carried out.

Availability of data and materials

The datasets used and/or analysed during the current study available from the corresponding author on reasonable request.

Conflict of Interests

The authors declare that they have no known competing financial interests or personal relationships that could have appeared to influence the work reported in this paper.

Funding

This work was supported by grants from the National Science and Technology Major Project for the Control and Prevention of Major Infectious Diseases in China (2018ZX10711001 and 2018ZX10102001) and the research start-up fund of the Second Affiliated Hospital of Nanchang University (B2117).

Authors' contributions

DS Yu, SH Yao, WN Xi, LF Cheng, FM Liu, HB Hu, XY Lu and HP Yao performed the experiments. HP Yao, DS Yu performed the statistical analysis. HP Yao, DS Yu, NP Wu and SL Sun designed the study and drafted the manuscript. All authors participated in writing the manuscript.

Acknowledgments

We sincerely thank the Cryo-Electron Microscopy Center of Zhejiang University for their help in the experiments.

References

1. Emond RT, Evans B, Bowen ET, Lloyd G: A case of Ebola virus infection. *British medical journal* 1977, 2(6086):541-544.

2. Kuhn JH: Guide to the Correct Use of Filoviral Nomenclature. *Current topics in microbiology and immunology* 2017, 411:447-460.
3. Agua-Agum J, Ariyarajah A, Blake IM, Cori A, Donnelly CA, Dorigatti I, Dye C, Eckmanns T, Ferguson NM, Fraser C *et al*: Ebola Virus Disease among Male and Female Persons in West Africa. *The New England journal of medicine* 2016, 374(1):96-98.
4. Keita M, Lucaccioni H, Ilumbulumbu MK, Polonsky J, Nsio-Mbeta J, Panda GT, Adikey PC, Ngwama JK, Tosalisana MK, Diallo B *et al*: Evaluation of Early Warning, Alert and Response System for Ebola Virus Disease, Democratic Republic of the Congo, 2018-2020. *Emerging infectious diseases* 2021, 27(12):2988-2998.
5. Lang HJ, Fontana L, Lado M, Kojan R: Triage of patients with Ebola virus disease. *The Lancet Infectious diseases* 2022, S1473-3099(22)00721-6.
6. Jackson WT: Viruses and the autophagy pathway. *Virology* 2015, 479-480:450-456.
7. Parzych KR, Klionsky DJ: An overview of autophagy: morphology, mechanism, and regulation. *Antioxidants & redox signaling* 2014, 20(3):460-473.
8. Levine B, Kroemer G: Autophagy in the pathogenesis of disease. *Cell* 2008, 132(1):27-42.
9. Choi AM, Ryter SW, Levine B: Autophagy in human health and disease. *The New England journal of medicine* 2013, 368(19):1845-1846.
10. Madrigal-Matute J, Cuervo AM: Regulation of Liver Metabolism by Autophagy. *Gastroenterology* 2016, 150(2):328-339.
11. Kaushik S, Cuervo AM: Chaperone-mediated autophagy: a unique way to enter the lysosome world. *Trends in cell biology* 2012, 22(8):407-417.
12. Sahu R, Kaushik S, Clement CC, Cannizzo ES, Scharf B, Follenzi A, Potolicchio I, Nieves E, Cuervo AM, Santambrogio L: Microautophagy of cytosolic proteins by late endosomes. *Developmental cell* 2011, 20(1):131-139.
13. Bandyopadhyay U, Cuervo AM: Entering the lysosome through a transient gate by chaperone-mediated autophagy. *Autophagy* 2008, 4(8):1101-1103.
14. Bandyopadhyay U, Kaushik S, Varticovski L, Cuervo AM: The chaperone-mediated autophagy receptor organizes in dynamic protein complexes at the lysosomal membrane. *Molecular and cellular biology* 2008, 28(18):5747-5763.
15. Chiang HL, Terlecky SR, Plant CP, Dice JF: A role for a 70-kilodalton heat shock protein in lysosomal degradation of intracellular proteins. *Science (New York, NY)* 1989, 246(4928):382-385.
16. Sancak Y, Bar-Peled L, Zoncu R, Markhard AL, Nada S, Sabatini DM: Ragulator-Rag complex targets mTORC1 to the lysosomal surface and is necessary for its activation by amino acids. *Cell* 2010, 141(2):290-303.
17. Kroemer G, Marino G, Levine B: Autophagy and the integrated stress response. *Molecular cell* 2010, 40(2):280-293.
18. Liang J, Sagum CA, Bedford MT, Sidhu SS: Chaperone-Mediated Autophagy Protein BAG3 Negatively Regulates Ebola and Marburg VP40-Mediated Egress. 2017, 13(1):e1006132.
19. Chiramel AI, Dougherty JD, Nair V, Robertson SJ, Best SM: FAM134B, the Selective Autophagy Receptor for Endoplasmic Reticulum Turnover, Inhibits Replication of Ebola Virus Strains Makona and Mayinga. *The Journal of infectious diseases* 2016, 214(suppl 3):S319-s325.
20. Yu DS, Weng TH, Hu CY, Wu ZG, Li YH, Cheng LF, Wu NP, Li LJ, Yao HP: Chaperones, Membrane Trafficking and Signal Transduction Proteins Regulate Zaire Ebola Virus trVLPs and Interact With trVLP Elements. *Frontiers in microbiology* 2018, 9:2724.
21. Hoenen T, Watt A, Mora A, Feldmann H: Modeling the lifecycle of Ebola virus under biosafety level 2 conditions with virus-like particles containing tetracistronic minigenomes. *Journal of visualized experiments : JoVE* 2014(91):52381.
22. Ramakrishnan MA: Determination of 50% endpoint titer using a simple formula. *World journal of virology* 2016, 5(2):85-86.
23. Mizushima N, Yoshimori T, Levine B: Methods in mammalian autophagy research. *Cell* 2010, 140(3):313-326.
24. Nanbo A, Imai M, Watanabe S, Noda T, Takahashi K, Neumann G, Halfmann P, Kawaoka Y: Ebolavirus is internalized into host cells via macropinocytosis in a viral glycoprotein-dependent manner. *PLoS pathogens* 2010, 6(9):e1001121.
25. Liang Q, Luo Z, Zeng J, Chen W, Foo SS, Lee SA, Ge J, Wang S, Goldman SA, Zlokovic BV *et al*: Zika Virus NS4A and NS4B Proteins Deregulate Akt-mTOR Signaling in Human Fetal Neural Stem Cells to Inhibit Neurogenesis and Induce Autophagy. *Cell stem cell* 2016, 19(5):663-671.
26. Mizushima N, Yamamoto A, Hatano M, Kobayashi Y, Kabeya Y, Suzuki K, Tokuhisa T, Ohsumi Y, Yoshimori T: Dissection of autophagosome formation using Apg5-deficient mouse embryonic stem cells. *The Journal of cell biology* 2001, 152(4):657-668.
27. Lee YR, Lei HY, Liu MT, Wang JR, Chen SH, Jiang-Shieh YF, Lin YS, Yeh TM, Liu CC, Liu HS: Autophagic machinery activated by dengue virus enhances virus replication. *Virology* 2008, 374(2):240-248.
28. Franke TF: PI3K/Akt: getting it right matters. *Oncogene* 2008, 27(50):6473-6488.
29. Mirzaa GM, Riviere JB, Dobyns WB: Megalencephaly syndromes and activating mutations in the PI3K-AKT pathway: MPPH and MCAP. *American journal of medical genetics Part C, Seminars in medical genetics* 2013, 163c(2):122-130.
30. Tekirdag K, Cuervo AM: Chaperone-mediated autophagy and endosomal microautophagy: Joint by a chaperone. 2018, 293(15):5414-5424.

31. Agarraberes FA, Dice JF: A molecular chaperone complex at the lysosomal membrane is required for protein translocation. *Journal of cell science* 2001, 114(Pt 13):2491-2499.

Tables

Table 1. TCID50 of trVLPs calculated by Reed-Muench method and conversion of MOI values.

Dilution of trVLPs	Counts of CPE wells	Counts without CPE wells	Accumulation of CPE wells	Accumulation without CPE wells	Percentage of CPE wells (%)
10^{-1}	7	1	18	1	94.7 18/19
10^{-2}	5	3	11	4	73.3 11/15
10^{-3}	3	5	6	9	40.0 6/15
10^{-4}	2	6	3	15	16.7 3/18
10^{-5}	1	7	1	22	4.3 1/23
10^{-6}	0	8	0	30	0 0/31
10^{-7}	0	8	0		

Cytopathic effect= (73.3-50)/ (73.3-40) =23.3/ 33.3= 0.70

lgTCID50=0.70× (-2) + (-2) = -3.4

TCID50=10E-3.4/ 0.1ml

MOI= TCID50×0.7/cell numbers =TCID50×0.7/10000 cells= 0.20

Table 2. Information of siRNAs chosen for RNA interference experiments.

NO.	siRNAs (product name)	Product Id	siRNA Target Sequence	Ct（primer（gene）	Ct（primer（18s）	ΔCt	-ΔΔCt	$2^{-\Delta\Delta Ct}$
1	negative control			27.86	15.81	12.05		
	Hs_HSC70	SI04213370	GAGGTTGATTAAGCCAACCAA	28.85	14.89	13.96	-1.91	0.2660925
2	negative control			36.4	13.67	22.73		
	Hs_HSPA1A	SI04364136	TCCGGTTTCTACATGCAGAGA	37.42	14.78	22.64	0.09	1.0643702
3	negative control			21.6	13.27	8.33		
	Hs_HSP90AB1	SI02780561	CAAGAATGATAAGGCAGTTAA	22.8	14.18	8.62	-0.29	0.8179021

Figures

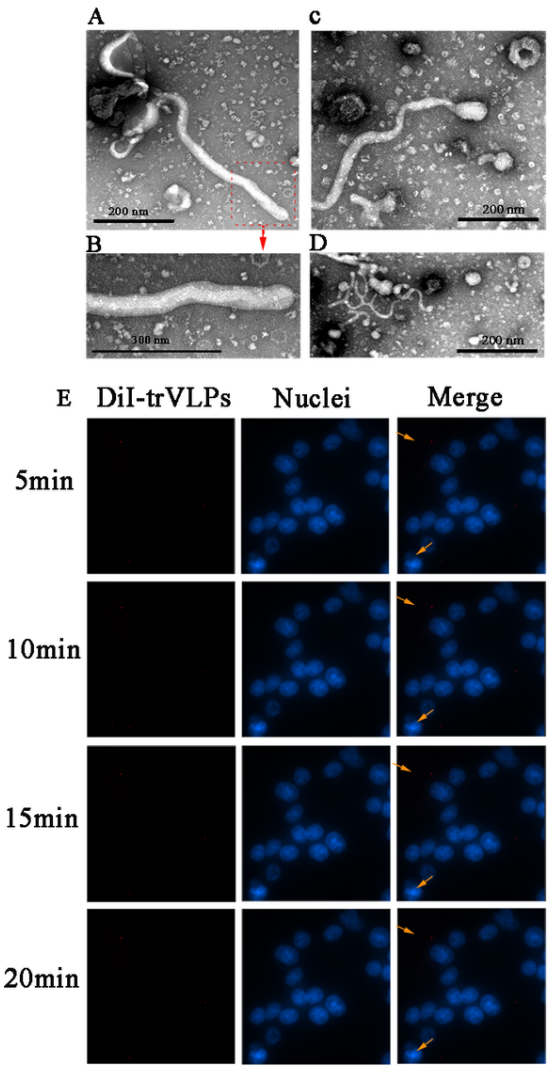

Figure 1

Production of EBOV-trVLPs. (A-D) Visualization of EBOV-trVLPs by EM. trVLPs were produced according to the protocol, purified by ultracentrifugation using a 20% sucrose gradient, and virion particles were visualized by EM following negative staining. The trVLPs exhibit filamentous-like viral particles. (E) Cellular internalization of DiI-labeled trVLPs. trVLPs were added to DiI label, which could be traced by fluorescence microscopy. At 5, 10, 15, and 20 min after 293T cells were infected, the DiI-trVLPs shows the activity of the invading cells (indicated by yellow arrows). EBOV-trVLPs, ebolavirus transcription- and replication-competent virus-like particles; EM, electron microscopy; DiI, 1,1'-dioctadecyl-3,3,3',3'- tetramethyl indocarbocyanine perchlorate.

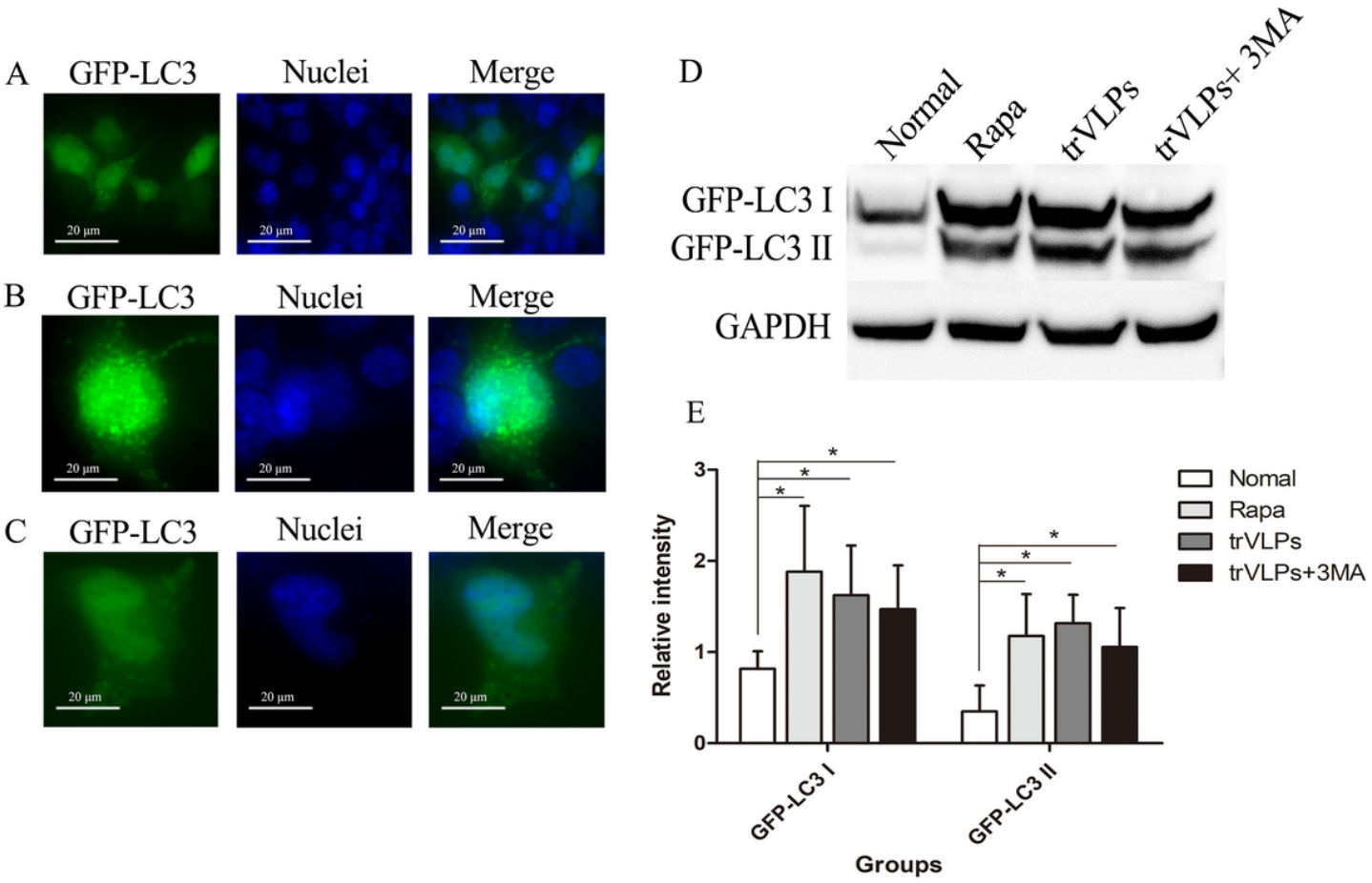

Figure 2

EBOV-trVLPs induce autophagy. (A) At 48 h post-trVLPs infection, autophagy was observed in 293T cells. GFP-LC3 punctate structures in the cells represent autophagosome numbers. (B and C) At a high magnification, rich GFP-LC3 punctate dots (³ 5 dots/cell) are used to monitor autophagosome numbers in GFP-LC3-transfected cells. (D) Immunoblot analysis of autophagy. The conversion from GFP-LC3-I to GFPLC3-II indicated autophagy. The results indicated that the cells induced by rapamycin or infected by trVLPs were associated with significant GFP-LC3-II expression. Cells previously treated with 3-MA and then later infected with trVLPs also exhibited obvious GFP-LC3-II expression, which suggested that 3-MA could not effectively inhibit trVLPs-induced autophagy.

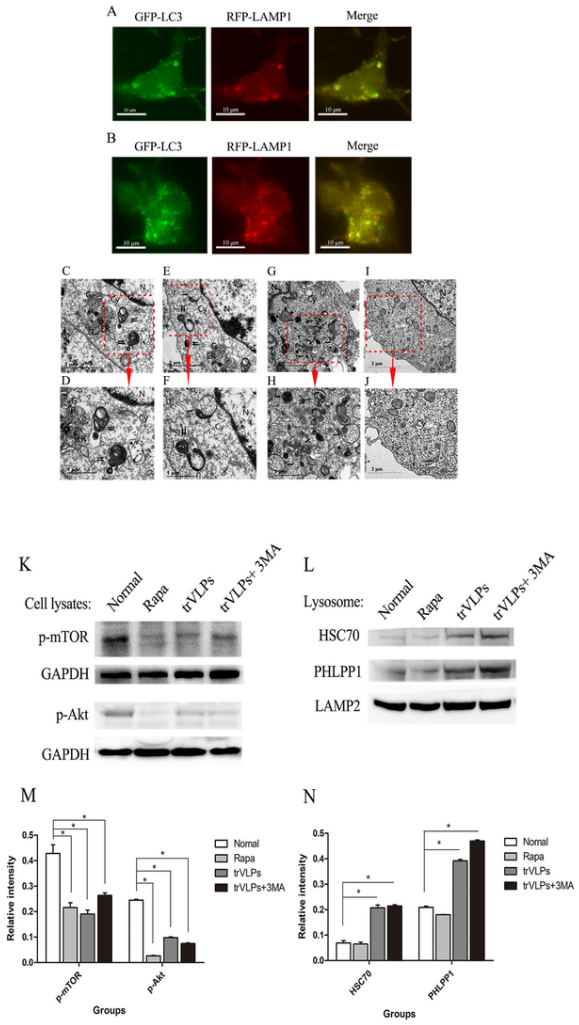

Figure 3

EBOV-trVLPs induced autophagy via the CMA pathway. (A and B) Co-localization of RFP-LAMP1- and GFP-LC3-positive dots (yellow) indicate autolysosomes. The 293T cells previously transfected with GFP-LC3 and RFP-LAMP1 were infected by EBOV-trVLPs for 48 h. RFP-LAMP1-positive dots (red) represent lysosomes and autophagolysosomes; GFP-LC3-positive dots (green) represent autophagosomes and autolysosomes. Thus, the co-localization of autophagosomes and autolysosomes is indicative of autolysosomes, which implies autophagy maturation induced by the CMA pathway. (C - F) Autophagosome and autolysosome morphology assessed by TEM. According to the protocol, 293T cells were infected with trVLPs for 48 h, then observed under TEM after sample preparation. In the images, autophagosomes (indicated by a single arrow) and autolysosomes (indicated by double arrows) are obviously visible in the cytoplasm. Panel F clearly shows an autophagosome fusing with a lysosome to form an autolysosome (indicated by double arrows). (G and H) 293T cells treated with rapamycin were used as a positive control. Autophagosomes (indicated by a single arrow) are richly expressed in the cytoplasm. (I and J) Normal 293T cells were treated as the negative control. (K) Immunoblot analysis of the level of cellular P-mTOR and P-Akt after infection with trVLPs. P-mTOR and P-Akt from the cell lysates were significantly lower in the cells treated with trVLPs or rapamycin or trVLPs plus 3-MA compared to the normal cells. Moreover, there were no distinct changes in P-mTOR or P-Akt expression between the groups treated with trVLPs and trVLPs plus 3-MA. (L) Immunoblot analysis of lysosomal HSC70 and PHLPP1 following infection with trVLPs. HSC70 and PHLPP1 were enriched in both the trVLPs and trVLPs plus 3-MA groups, but were thin in the rapamycin and normal groups. The lysosomal protein, LAMP2, was used as the internal control. Cy, cytoplasm; ER, endoplasmic reticulum; G, Golgi apparatus; N, nuclei.

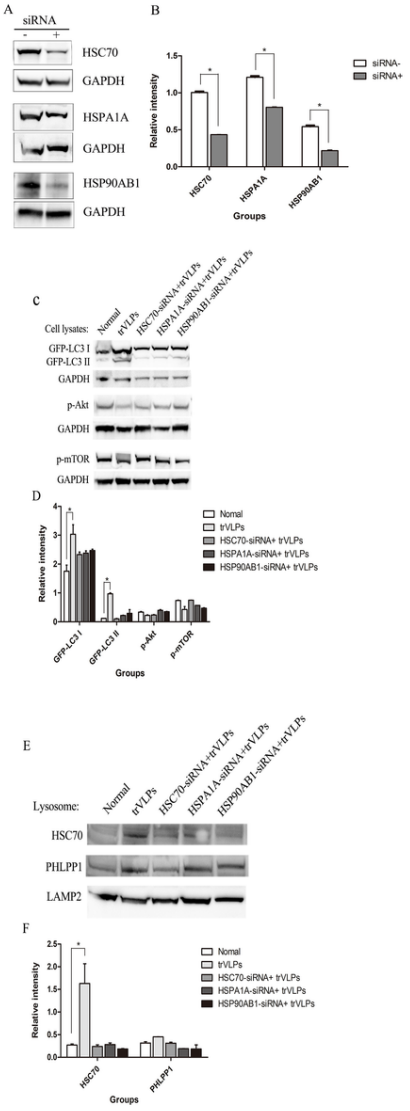

Figure 4

Downregulation of HSC70 and co-chaperones could affect trVLPs-induced CMA. (A) Western blot analysis of the target protein following siRNA transfection. HSC70, HSPA1A, and HSP90AB1 all exhibited a much lower expression after transfection with relevant siRNA compared with cells without siRNA interference. (B) An immunoblot analysis of cellular GFP-LC3, P-mTOR, and P-Akt following transfection of siRNA and infection with trVLPs. According to the protocol, the cells were previously transfected with siRNA and infected with trVLPs for 48 h. Knockdown of HSC70, HSPA1A, and HSP90AB1 could substantially inhibit the conversion of GFP-LC3-I to GFP-LC3-II, but had little effect on P-mTOR and P-Akt expression. (C) Immunoblot analysis of lysosomal HSC70 and PHLPP1 following siRNA transfection and trVLPs infection. Knockdown of HSC70, HSPA1A, and HSP90AB1 could eliminate lysosomal HSC70 expression, but had no effect on lysosomal PHLPP1. Lysosomal protein LAMP2 was used as an internal control.

Supplementary Files

This is a list of supplementary files associated with this preprint. Click to download.

- SupplementaryFigure1.docx